Lab on a Chip

Patterned Thin Film Enzyme Electrodes via Spincoating and Glutaraldehyde Vapor Crosslinking: Towards Scalable Fabrication of Integrated Sensor-on-CMOS Devices

Journal:	*Lab on a Chip*
Manuscript ID	LC-ART-03-2024-000206.R1
Article Type:	Paper
Date Submitted by the Author:	26-Jun-2024

Complete List of Authors:	Adalian, Dvin; California Institute of Technology, Madero, Xiomi; California Institute of Technology Chen, Samson; California Institute of Technology Jilani, Musab; California Institute of Technology Smith, Richard; California Institute of Technology Li, Songtai; California Institute of Technology Ahlbrecht, Christin; Helmholtz Zentrum Munchen Deutsches Forschungszentrum fur Gesundheit und Umwelt Cardenas, Juan; California Institute of Technology Agarwal, Abhinav; California Institute of Technology Emami, Azita; California Institute of Technology Plettenburg, Oliver; Helmholtz Zentrum Munchen Deutsches Forschungszentrum fur Gesundheit und Umwelt Petillo, Peter; Design-Zyme LLC Scherer, Axel; California Institute of Technology

ARTICLE

Patterned Thin Film Enzyme Electrodes via Spincoating and Glutaraldehyde Vapor Crosslinking: Towards Scalable Fabrication of Integrated Sensor-on-CMOS Devices

Accepted 00th January 20xx

DOI: 10.1039/x0xx00000x

Dvin Adalian*[a], Xiomi Madero[a], Samson Chen[a], Musab Jilani[a], Richard D. Smith[a], Songtai Li[a], Christin Ahlbrecht[b], Juan Cardenas[a], Abhinav Agarwal[a], Azita Emami[a], Oliver Plettenburg[b], Peter A. Petillo[c], Axel Scherer[a]

Effective continuous glucose monitoring solutions require consistent sensor performance over the lifetime of the device, a manageable variance between devices, and the capability of high volume, low cost production. Here we present a novel and microfabrication-compatible method of depositing and stabilizing enzyme layers on top of planar electrodes that can aid in the mass production of sensors while also improving their consistency. This work is focused on the fragile biorecognition layer as that has been a critical difficulty in the development of microfabricated sensors. We test this approach with glucose oxidase (GOx) and evaluate the sensor performance with amperometric measurements of in vitro glucose concentrations. Spincoating was used to deposit a uniform enzyme layer across a wafer, which was subsequently immobilized via glutaraldehyde vapor crosslinking and patterned via liftoff. This yielded an approximately 300 nm thick sensing layer which was applied to arrays of microfabricated platinum electrodes built on blank wafers. Taking advantage of their planar array format, measurements were then performed in high-throughput parallel instrumentation. Due to their thin structure, the coated electrodes exhibited subsecond stabilization times after the bias potential was applied. The deposited enzyme layers were measured to provide a sensitivity of 2.3 ± 0.2 μA/(mM·mm^2) with suitable saturation behavior and minimal performance shift observed over extended use. The same methodology was then demonstrated directly on top of wireless CMOS potentiostats to build a monolithic sensor with similar measured performance. This work demonstrates the effectiveness of the combination of spincoating and vapor stabilization processes for wafer scale enzymatic sensor functionalization and the potential for scalable fabrication of monolithic sensor-on-CMOS devices.

Introduction

The development of continuous glucose monitors (CGMs) has transformed how patients with diabetes measure their serum glucose levels in non-clinical settings[1,2]. Despite the numerous advances that have been made to support the widespread consumer acceptance of this monitoring modality, there continues to be a need for further improvement, particularly for longer-term, lower-impact body integration[3–8]. Transdermal and centimeter-scale wireless devices have been observed to be lifetime-limited by rejection, but these formats are the current state of the art for scalable device fabrication[9,10]. Implementing complete miniaturized implantable-scale sensor construction via microfabrication methodologies could lead to both desired lower costs and less immune rejection.

The recent development of monolithically integrated CMOS-based wireless potentiostats[11] is the foundation that could permit unprecedented fabrication throughput for biosensors by replacing traditional multiple-component assembly with parallelized, wafer-scale sensor fabrication. Via this approach, it becomes possible for a single CMOS wafer to provide tens of thousands of wireless glucose monitors with high fabrication uniformity. However, the scalable incorporation of the biorecognition element is a remaining challenge to permitting full sensor stack microfabrication via wafer-scale processes.

By adopting a planar sensor geometry one can take advantage of the array of existing microfabrication techniques to construct both an enzyme layer and the underlying transduction element. Spincoating is one such process that enables deposition of molecules with the scale and structure of enzymes uniformly over a wafer. This technique has been used to deposit enzymes on rotating disc electrodes for analytical kinetic studies[12–14], but patterning is either nonexistent or limited to radial symmetry in such experiments. Spincoating combined with patterning of enzymes has been previously described[15–18], but those implementations did not demonstrate either the analyte sensitivity, parallel sensor construction or reproducibility, necessary to permit consistent lot-to-lot fabrication with suitable performance. Here we report on our efforts to utilize enzyme spincoating with a vapor-deposited crosslinker as a method to construct arrays of enzymatic biosensors across a flat

[a] California Institute of Technology, Pasadena, CA 91125, United States
[b] Helmholtz Zentrum Munchen Deutsches Forschungszentrum fur Gesundheit und Umwelt, Institute of Medicinal Chemistry, Hannover, 30167, Germany
[c] Design-Zyme LLC, 4950 Research Park Way, Lawrence, Kansas 66047, United States

planar geometry in a manner compatible with large scale fabrication.

The essential objective to developing our deposition process is compatibility with CMOS foundry wafers and the target implant in vivo environment, and while functional techniques already exist for non-monolithic sensing electrodes, such as in wire/needle-type devices, they have inherent drawbacks for wafer-level processing of monolithic devices[19]. Screen-printing scales readily, but does not have the resolution to take advantage of the potential density of CMOS fabrication[20]. Electrodeposition can produce both highly electrically conductive and high selective chemical activity layers that retain and protect enzymes, but the deposition requires additional driving circuitry beyond a measurement potentiostat which is difficult to incorporate to scaled device fabrication of this type[21–23]. 2nd generation format sensors can address the in vivo problems with oxygen consumption, but require a mediator that is not likely to stay contained long-term to the device[19]. Nonzymes can in principle alleviate the problems with enzyme longevity, but so far have issues with stability and applicability in an in vivo environment. The relatively new category of CMOS-scale biosensors with its potential advantages, is best served by the well employed technique for planar devices of spincoating.

It is common in the construction of glucose sensors to combine a glucose responsive enzyme with bovine serum albumin (BSA) before crosslinking via glutaraldehyde (GA) to create a stabilizing retention matrix for the enzyme[3,24]. Enzyme mixtures have been deposited onto the sensor transduction elements by a variety of methods such as drop-casting, dipcoating, or inkjet printing in both academic research and industry. In undertaking this work, we sought to leverage the already known stability of GOx-BSA-GA chemistry in a new scheme amenable to microfabrication scaling. We then analyzed what improvements could occur for the consistency and performance properties due to this process.

Two performance benefits that we anticipated were increased current-per-analyte-consumed efficiency and decreased concentration determination time. Traditional deposition techniques unavoidably result in either non-uniform or micron-thick enzyme layers because of the high and dynamically increasing viscosity of enzyme deposition mixtures already containing an active polymerizer and Marangoni effects. However, the external side of the enzyme immobilization layer, closest to the environmental analyte, will perform more of the H_2O_2 generating reaction[25] and thus shrinking the distance to the transduction electrode would directly aid in the H_2O_2 capture efficiency, reducing the likelihood of the H_2O_2 diffusing away or reacting extraneously relative to electrode interaction. A thinner enzyme layer would also increase the sensor response speed during a measurement because the layer will more quickly come to equilibrium with changes in the environment due to the shorter diffusion distance.

Although spincoating is a well-studied and broadly utilized process within semiconductor microfabrication, successful adaptation of this technique to biosensor fabrication requires determining which steps are compatible with the enzyme molecules or need novel solutions. Further, we observed that the direct employment of a premixed GOx-BSA-GA solution could not provide a well-behaved result for submicron layers.

While depositing the enzyme solution under various conditions across 100 mm wafers it was observed that the crosslinking reaction cannot be controlled with sufficient fidelity to permit uniform production of the enzyme immobilization layer within a wafer and across batches. The reaction produced particles and viscosity fluctuations which interfered with spincoat uniformity. The process was sensitive to ambient temperature and humidity effects, and controlling these factors in a manufacturing environment to the necessary extent would be burdensome. As such, we chose to remove the crosslinking agent until after the spincoating, by adapting a method described by Salem et al.[26] where vapor deposition of GA led to successful results with their immobilization geometry.

This alternative process was used to form thin enzyme layers across wafers with micropatterned electrodes that were wired for external electrical probing while submerged in analyte solution. After initial fabrication of the electrodes, a GOx-BSA-PBS mixture was spincoated onto the sensor surfaces, and then exposed to GA vapor in a low vacuum chamber to generate an immobilized, crosslinked structure. This two-step deposition approach enabled the reliable deposition of enzyme layers with average thicknesses below 500 nm. The enzyme layers were then evaluated by electrochemical measurements for magnitude, speed, and lifetime. A performance comparison is provided here between dropcoat and spincoat type sensors as well as multiple spincoat sensor batches. An additional consequence of transitioning to spincoat deposition was successful integration with a photoresist sublayer which enabled patterning the enzyme coatings to the selected electrodes. This enables precise lateral control of the enzyme coating for each electrode, which improves the consistency of wafer-scale device production. This approach is then successfully implemented on top of a wireless CMOS potentiostat, yielding similar functionality in a millimeter-scale device. Based on the observed performance, this thin sensor architecture can be a solution for enzyme-functionalization of future dense, large-area wafer device arrays in high volume, cost-efficient fabrication.

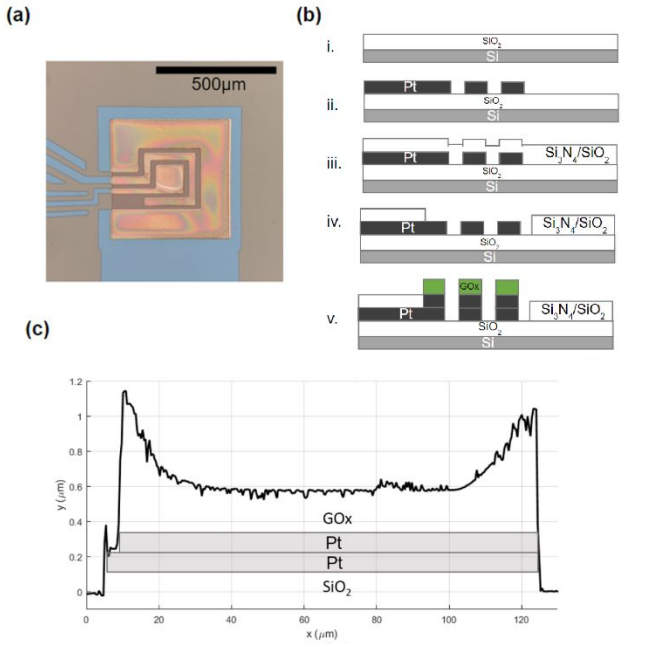

Figure 1. (a) Wired sensor with three platinum electrodes and patterned GOx coating. Electrodes in order from center outwards: WE, RE, CE. Blue regions are connection traces covered by Si_3N_4/SiO_2 insulation. (b) Silicon wafer fabrication sequence: (i.) thermal oxidation (ii.) patterned platinum deposition and liftoff (iii.) PECVD Si_3N_4 and SiO_2 (iv.) plasma etching (v.) platinum evaporation onto patterned resist followed by GOx spincoat and liftoff. (c) 2D AFM scan of a patterned working electrode Enzyme Concentration A spincoat after liftoff. Accumulation at the spincoat edges is visible.

Experimental

Reagents and materials

Glucose Oxidase from Aspergillus niger was purchased from BBI Solutions (#GO3A). Bovine serum albumin (AMRESCO # 97064-340) and 10X Phosphate Buffer Saline, Molecular Biology Grade (Corning #46-013-CM) were purchased from VWR. D-(+) Glucose (Sigma #G8270) and 25% Glutaraldehyde, electron microscopy grade (ACROS #23328) were also purchased from VWR. Sodium Benzoate 99.0 % (ACROS #AC148980010) was purchased from Fisher Scientific. Phosphate-buffered saline solutions were diluted using deionized water (resistivity 18.0 MΩ·cm) filtered through 0.22 µm pores (Durapore #CVDI02TPE) and UV sterilized (Aquafine). MicroChemicals AZ 5214-IR was the main photoresist used.

Titanium (99.99%) and platinum (99.99%) were purchased from Kurt J. Lesker Company. 100 mm silicon wafer substrates were utilized from a variety of sources as they are used only as a platform. CMOS wafers were manufactured by TSMC and procured via MOSIS's MPW service.

Instrumentation

Microfabrication of the three-electrode platinum planar sensors (Fig. 1a) was performed with standard photolithography tooling, and depositions were performed with a CHA Industries Mk40 electron beam evaporator or AJA ATC Orion 8 sputter system utilizing an IC/5 Inficon deposition control and quartz crystal thickness monitor. Silicon oxidation was performed with a Tystar Tytan furnace. Trace line insulation layers were built and patterned using an Oxford PlasmaPro 100 PECVD and an Oxford ICP PlasmaPro 380 RIE respectively.

A Laurell WS-400 Spin Coater was used for the application of GOx-containing solution to the wafers. GA deposition was performed with a hot plate contained in a bell jar. Thickness measurements were carried out on the wafer with a Dektak XT Stylus profilometer and Bruker Dimension Icon AFM.

All wired wafer electrochemical experiments were performed with Keithley Instruments 2450 SourceMeters operating in 3-electrode potentiostat mode. The finalized sensors were evaluated in a custom built fluidic cell system with centralized control of potentiostat reading and analyte concentration delivery to each cell. (Fig. 2a) Wireless electrochemical measurements were performed with an on-board CMOS potentiostat as described in Agarwal et al.[27] and devices were communicated with through the wall of a beaker.

Wafer-Scale Processing of Electrode Sets

Micropatterned electrodes were built in a cleanroom environment using standard thin film patterning techniques (as shown in Fig. 1b). For sensors starting from a bare silicon substrate, the wafer was first thermally oxidized at 1000 °C to grow a 2.5 µm thick layer for isolating the metallic sensors from each other and the substrate. Standard photoresist processes were used for sensor patterning. A first metal layer was deposited to define the working electrode (WE), counter electrode (CE), reference electrode (RE), connections between the electrodes and the probe pads. This consisted of a 10 nm Ti adhesion layer and a 100 nm Pt surface layer, which were deposited by electron beam evaporation or sputtering and isolated via liftoff. Next, a 240 nm thick layer of SiO_2 and 30 nm of Si_3N_4 were deposited via PECVD, in order to insulate the trace lines from the cell solution. Openings for the defined electrode areas and probe pads were generated by photolithography and fluorine-based plasma etching. Subsequent metal layers for the electrodes were added in a manner similar to the first layer in order to implement an electrode material, thickness, and/or surface morphology of choice. Enzyme spincoating was trialed in both complete wafer coatings and patterned coatings. In the latter case, prior to enzyme spincoating, a photoresist mask was patterned to constrain the functionalized region over three separate electrodes within a 500 µm square of uninsulated electrode surface. This pattern was also used to deposit an additional layer of platinum over the electrodes before the enzyme deposition such that they only coated the three initially defined electrodes after a solvent liftoff process. Pattering the enzyme coating simplified the dicing process for the CMOS sensor version and aids compatibility with any future microfabrication step choices. For comparison, dropcoat-type

ARTICLE

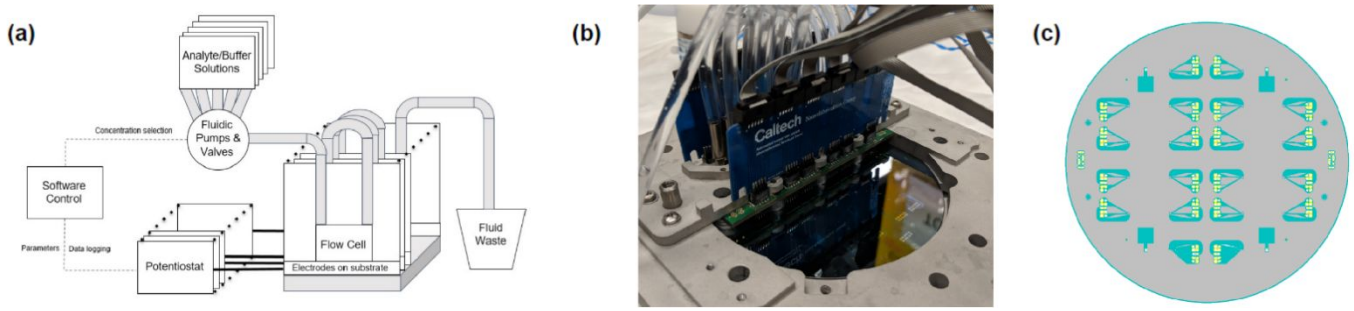

Figure 2. (a) Schematic of the wafer measurement station for routing fluidics and electrical connections to planar electrode sets. (b) Wafer loaded into the measurement station with electrodes and fluidics mounted. (c) 100 mm wafer electrode layout.

wafers were also fabricated with platinum electrodes deposited in the same mask configuration but with no enzyme patterning. The coating geometry relied on a syringe process described below.

CMOS post-processing was done at a 50 mm substrate scale due to tool limitations. The sensor fabrication process is parallel to the 100 mm silicon dioxide wafer process except that the electrodes were connected to CMOS contact pads instead of deposited on blank substrate.

Platinum was chosen as the electrode material as it provides a well examined[28] and high activity for H_2O_2 oxidation reaction at the WE[29]. Pt also performs well as a CE with H_2O_2 or O_2 reduction providing the counter-current. However, the CE will be substantially polarized necessitating the use of a separate RE. Since all measurements were performed in well-oxygenated PBS solutions with H_2O_2 available for oxidation and reduction as well, a Pt RE can also perform with suitable stability, thus simplifying the fabrication process.

Electrode Functionalization

The enzyme layer solution for spincoating one wafer was prepared with two concentration procedures. Enzyme Concentration A was 0.56 g of GOx and 0.47 g of BSA dissolved in 7 ml of 1X PBS solution and Concentration B was 0.96 g of GOx and 0.80 g of BSA dissolved in 6 ml of 1X PBS solution. The enzyme solution was vortexed for 30 s and centrifuged for 1 min and then passed through a 0.22 µm filter. The entire filtered solution was dispensed with a plastic pipette onto the wafer centered on the spinner and spin-coated at 500 rpm for 10 s followed by 4000 rpm for 30 s. The coated wafer was then placed on a thermally isolated mount within a chamber evacuated to -70kPA with an open vessel of GA heated to 80 °C for 7.5 minutes to complete the GA vapor deposition crosslinking.

Drop coating was tested as a deposition method for the comparison wafer sensors as informed by Koudelka-Hep et al.[30]. A 20 µl GOx-BSA solution consisting of 1.6 mg of GOx and 1.3 mg of BSA in 1X PBS was vortexed for 15 s and then centrifuged for 15 s. 25 % GA was then diluted 10:1 with 1X PBS. 6 µl of the GOx /BSA solution was mixed with 2 µl of GA and then vortexed for 5 s and centrifuged for 5 s, while seeking to minimize the amount of time before final deposition in order to prevent premature polymerization. The sensing layer was then applied by dispensing 1 µl of the GOx-BSA-GA solution via pipette onto the electrodes. Beginning room temperature polymerization before final deposition requires consistent timing in order to obtain good reproducibility with this deposition method.

Electrode Geometry

Twenty 3-electrode sensors were built per blank wafer, evenly distributed over the surface as in the diagram Fig. 2c. The platinum WE was patterned at 0.0182 mm^2, partially encircled by an RE and CE within a total area of 500 µm x 500 µm. Fig. 1a shows the typical geometry of the potentiostat electrodes.

For the CMOS samples the total electrode area was 825 µm x 825 µm and Fig. 5a shows a typical geometry for the fabricated electrodes.

Experimental Measurement and Analysis Methods

Completed wired sensor wafers were loaded into a custom probe system to provide voltage control to the WE, CE, and RE via the potentiostat instruments. The probe system utilizes an array of aligned and o-ring sealed wet cells for delivering varied concentrations of glucose to independently measured electrode sets across a wafer (Fig. 2b). These cells are serially connected by tubing in order to reduce the complexity of the external solution delivery system. Solutions of 1X PBS with 0.1

ARTICLE

% w/v sodium benzoate and clinically relevant glucose concentrations were manually prepared and automatically delivered in randomized sequences to all cells simultaneously at local room temperature (22-24°C). For interference studies, ascorbic acid and uric acid were also added to the testing solutions. Two different measurement protocols were employed, a static measurement and a 'flow' measurement. In both, the 6 µl cell is flushed by 60 ml of the next concentration solution. In the static observation the flow is paused and after a 5 second delay, a 60 second data recording begins, sampled at 0.1 s intervals. In the 'flow' measurement, the 60 second measurement period runs while the pump is active in order to better discern the transport contributions of the enzyme layers from that of the wet cell by bringing an effectively constant concentration boundary condition closer to the film. This causes a reduced duration for external diffusion time contributions and also prevents analyte depletion or product buildup, though it also modifies the current-concentration relationship compared to when a static diffusion over-layer is used. Each concentration is delivered 4-8 times in randomized sequences to eliminate error biases due to hysteretic effects. The measurement sweeps through multiple concentrations and iterations typically ran for 1 to 2 hours. Afterwards the electrode sets were maintained in room temperature PBS until the next measurement round.

Wireless CMOS electrode measurements were performed with the same solutions loaded into 10 ml beakers. Concentrations were sorted by random and measurements were performed for 1-2 minutes. Current data were collected via custom RF antenna hardware and software.

During measurement, the WE is set to +0.4 V versus the platinum RE of the same sensor[31]. Under these environmental conditions, this bias is similar to the typical practice of applying +0.65 V versus an Ag/AgCl reference electrode in saturated KCl solution, as informed by both expected platinum redox behavior and verification with a Ag/AgCl electrode. As the Pt electrode is both well oxygenated in vitro and has a source of H_2O_2, its open circuit potential is approximately +0.25 V relative to Ag/AgCl (in sat. KCl). The functionalization process for the WE can be easily separated from the RE/CE fabrication steps such that Pt layers without immobilization or other planar RE materials may be employed, but this was unnecessary for the purposes of this demonstration.

Fitting parameters are obtained via MATLAB for the response and saturation behavior of each sensor as the glucose concentration is increased. Michaelis-Menten (M-M) analysis traditionally provides a measure of how effectively product (H_2O_2 molecules) is generated from substrate, and is often employed as an 'apparent' approximation when measuring product at a practical working electrode which will experience transport, transduction, and interference losses that cause a mismatch from analytical enzymatic behavior in homogenous solutions[32]. An apparent k_m and production rate v_{max} or equivalent electrical current I_{max} are calculated via the Lineweaver-Burk which is a simplification to single-substrate kinetics but permits linear fitting of the data. An exponential curve-fit in Matlab is also employed to compare sensor data from similar diffusion/geometry conditions. The slope in the pre-saturation region of this exponential fit serves as thethe sensitivity (nA/mM) metric defined as $s = dV/d[S] \mid_{[S]=0}$., where s, V and [S] refer to the sensitivity, steady-state current, and glucose concentration, respectively. A limit of detection (LoD) is calculated based on the relative standard deviation (RSD) of the sensitivity factor but this only represents the capability of the enzyme layer without a linearizing flux-limiting layer.

Results and Discussion

The initial measurement sets were performed on the 100 mm wafers (of the pattern in Fig. 2c.) containing up to 20 probable wired sensors (of the type displayed in Fig. 1a). The thickness of the patterned spincoated Enzyme Concentration B layers was evaluated via profilometry on un-wired electrodes using an identical fabrication sequence as the wafers evaluated amperometrically (Fig. 1c). The average patterned Enzyme Concentration B layer thickness on the working electrodes when spinning Enzyme Concentration A was 390 nm with 128 nm standard deviation across the wafer. For comparison the dropcoat process produced layers with an average height of 32.3µm with 12.2µm standard deviation. For both approaches capillary effects at the edges create the largest nonuniformities but spincoating generates horizontal regions which is excluded by the coffee ring effect when dropcoating. After determining the performance properties of dropcoated and spincoated enzyme layers under static and 'flow' conditions on 100 mm wafers, the new spincoating recipe was applied to CMOS samples.

Wired Sensor Amperometric Response and Kinetics

Chronoamperometric measurements were performed on the wired wafer samples with iterated glucose concentrations, from which the steady-state signal and settling times were extracted. Manual photolithography errors caused some variance in the sensor yield per wafer. Current-concentration response curves are shown in Fig. 3a from measurement sweeps comparing the Enzyme Concentration B spincoated wafers. Table 1 lists the average and standard deviation of the kinetic and current values for the first round of measurements of the 16 sensors

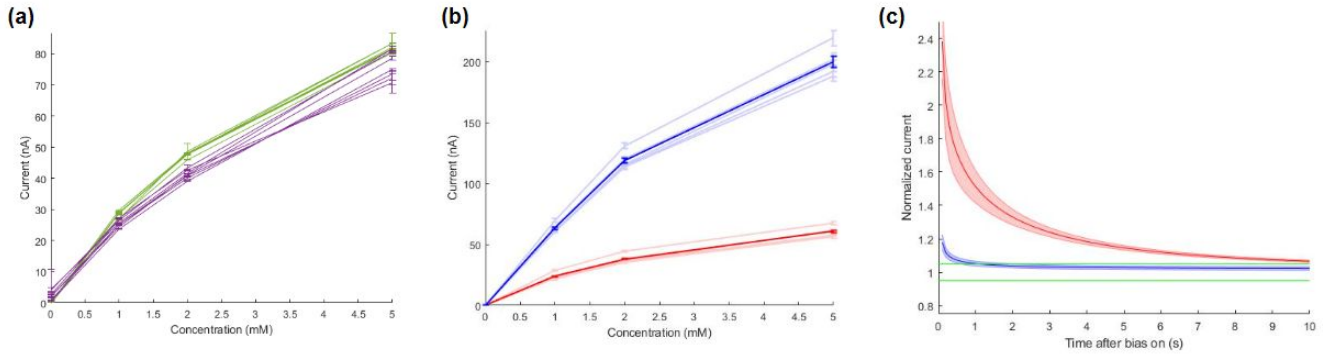

Figure 3 (a) Current-Concentration data from 8 wired sensors from two Enzyme Concentration B spincoat wafers (green and purple). (b) Current-Concentration data from 5 electrodes from Enzyme Concentration A spincoat (blue) and dropcoat (red) type wafers. An average of each sensor type's behavior is represented by the dark line while the faded lines show the data for each individual sensor. (c) Sensor stabilization comparison of dropcoat (red) and Enzyme Concentration A spincoat (blue) type electrodes within their first 10 seconds of bias. Green bounding bars represent 5 % deviation from the 60 second value. Normalizations are averaged over 5 electrodes of each type.

plotted via MATLAB in Fig. 3a for the two repeated wafers. The data displays that the same recipe conditions produced low-variance sensors within and across wafers. The glucose concentrations were also delivered with ascorbic acid and uric acid interferents at high-physiological concentrations (0.1 mM and 0.5 mM respectively) which produced 8% and 28% measurement error (against 3.9 mM glucose) which is in the expected range for a platinum electrode without an interferent barrier layer. A half-enzyme concentration spincoat (Wafer 3) generated a thinner enzyme layer which provides less signal than Enzyme Concentration B. Building thicker layers as in Spincoat Wafer 4 can provide more signal with diminishing returns in a closed fluid cell, but sacrifices equilibration speed.

Table 1 Average and standard deviation for the kinetic parameter, maximum current, sensitivity, and the limit of detection from the sensors in Fig. 3a of Enzyme Concentration B and comparison spincoat wafers in steady-state measurement

	k_m^{app} (mM)	I_{max} (nA)	Sensitivity (nA/mM)	LOD (mM)
Spincoat Wafer 1 (Enzyme Concentration B)	4.3 ± 0.4	151 ± 12	33.1 ± 2.6	0.26
Spincoat Wafer 2 (Enzyme Concentration B)	4.6 ± 0.7	141 ± 21	28.3 ± 1.8	0.22
Spincoat Wafer 3 (½ Enzyme Concentration B)	2.6 ± 0.4	71 ± 13	15.3 ± 2.2	0.47
Spincoat Wafer 4 (½ Spincoat RPM)	4.9 ± 0.9	163 ± 25	38.2 ± 2.8	0.24

A current-concentration response curve is shown in Fig. 3b from measurement sweeps under constant liquid flow for a spincoated wafer of Enzyme Concentration B and a dropcoated wafer. Measuring with continual fluid exchange highlights the diffusion dynamics within the compared layers relative to the dynamics in the fluid cell. Table 2 lists the average and standard deviation of the kinetic and current values for the first round of measurements of the 10 sensors plotted in Fig. 3b for the two sensor types. Thinner enzyme layers were able to transduce a larger portion of the analyte concentration in the same measurement time window. Within a daily measurement session with 40 solution variations, each electrode had an average measurement RSD of 1.2%. The two standard deviation confidence interval for the Lineweaver-Burk fit, primarily due to the oversimplification of the sensor transport/activity, was 8.9% and 8.2% for k_m and sensitivity respectively. Also due to the insuitability of M-M for immobilized enzymes, the sensor-to-sensor k_m RSD was 18% but the sensitivity RSD 3.2%

Table 2 Average and standard deviation for the kinetic parameter and maximum current from the sensor types in Fig. 3b under 'flow' conditions

	k_m^{app} (mM)	I_{max} (nA)
Spincoat Process	6.7 ± 1.4	465 ± 92
Dropcoat Process	3.2 ± 0.8	108 ± 24

Transient Behavior

In addition to increasing the sensor's response magnitude, reducing the thickness of the enzyme layer reduces the post-bias settling time of the sensor. This measurement is made under 'flow' conditions to avoid finite analyte diffusion cell behavior and extract the dynamics of the sensor when turned on. In thicker, drop-coat type sensors, we observed that the sensor response does not settle post-bias in less than 10 seconds, which may be due to the diffusion lengths of the analytes and products through the coating. However, in thin enzyme layers, we have observed that the in vitro stabilization delay can be greatly reduced to less than 0.5 seconds while maintaining high total current response. Thicker spincoats can

increase the current with diminishing returns but extends the stabilization time to multisecond. This difference is presented in Fig. 3c by plotting the transient current readings after the bias is applied for both thick (dropcoat) and thin (spincoat) enzyme layers. The current data across all time is normalized against the current value measured at 60 seconds after turning on the bias and displays a clear settling time reduction for thinner enzyme layers. With these curves, we can predict the settling time required to obtain a stable and accurate reading. However, defining a true steady-state is complex due to the nature of the platinum reaction and limitations of building a small volume diffusion cell. In contrast to an in vivo environment, under static conditions the in vitro cell used for the wired wafer samples will eventually deplete of reactants, causing the current to drop, which may occur before a relatively slow sensor has reached a steady-state.

Sensor Lifetimes

The sensor lifetime and deterioration rate are also critical aspects for CGMs. Toward this end, we investigated our wired in vitro sensor lifetimes by performing measurement sweeps under 'flow' conditions over the course of 40 days. New glucose solutions were mixed each measurement day. Fig. 4a shows the slow drift of the sensitivity and k_m during this time period. The sensor parameters remained viable during this period and exhibited a steady mild decay and there was no indication of an impending dramatic degradation toward the end of the measurement period. The addition of a flux limiting membrane would stabilize the k_m over the functional life of the sensor by reducing sensitivity to changes in cofactor concentration or other environmental factors[21], but this work is focused solely on the properties of the enzyme layer. As a result, the linear concentration regime is smaller than clinically relevant as that is typically extended by the flux limiting layer. Overall, these k_m ranges agree with prior reported in vitro GOx on Pt measurements[33].

We have also examined the change in signal settling over long-term measurements and observed improved consistency with spincoat sensors compared to dropcoat sensors as shown in Fig. 4b.

(a)

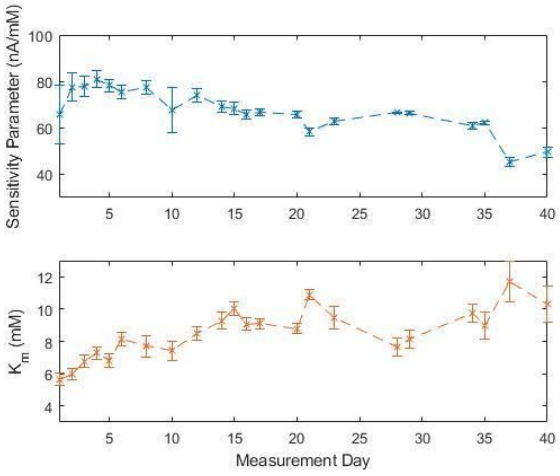

(b)

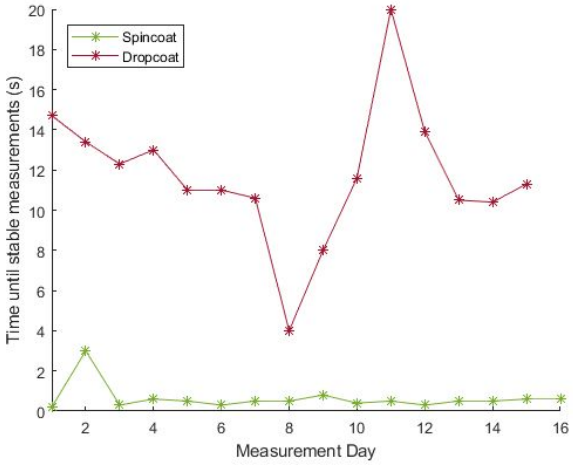

Figure 4 (a) Sensitivity and k_m over 40 days of measurements, averaged over 5 electrodes. (b.) Settling times for dropcoat-type and spincoat-type wired sensors over the course of 16 days.

Wireless CMOS Sensor Amperometric Response and Kinetics

After several experimental sequences verifying the functionality of the 100 mm wafer-fabricated sensor, an analogous structure was microfabricated onto CMOS substrates. Chronoamperometric measurements were also performed on these integrated devices (shown in Fig 5a before dicing) with randomly delivered glucose concentrations. The calculated k_m^{app} and I_{max} at the 2 second mark are 7.1 ± 1.6 mM and 131 ± 25 nA, respectively and at the final measurement time 8.1 ± 2.3 mM and 149 ± 33 nA respectively. These results demonstrate similar performance to sensors built on the wired sensor platform and confirm the applicability of this fabrication process to its final device goal.

(a)

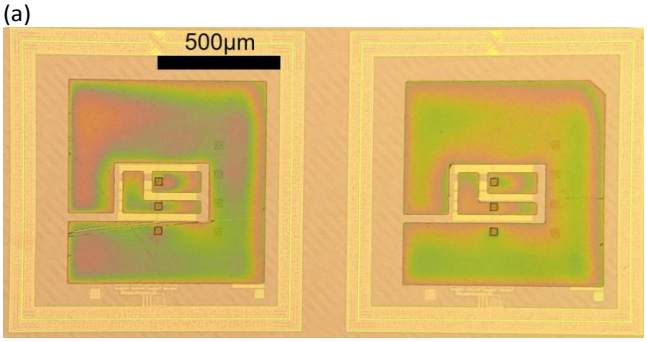

(b)

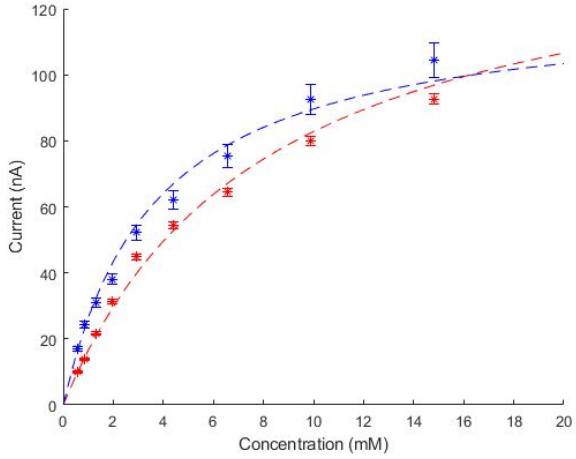

Figure 5 (a) Two wireless CMOS three-electrode platinum patterned GOx coated sensors. (b) Current-Concentration data with km fit curves from a wireless CMOS device with Enzyme Concentration B at 2 second measurement time (Blue) and final time (Red).

Review

Employing thin, spincoated enzyme layers on electrochemical glucose sensors shows distinct performance advantages while also prompting novel device design considerations. Patient treatment could be improved by using layers with faster equilibration dynamics, as their shorter delays and better temporally resolved measurements allow for more accurate and frequent readings[34]. For miniaturized sensors the total and continuous energy requirements could be reduced through the ability to briefly pulse measurements that rapidly settle after biasing. This would be distinct from other devices which must be left on due to the relatively slow diffusion dynamics through their layers. Since the in vivo dynamics of the glucose concentration are expected to be much slower than a pulsing frequency set by the enzyme layer transient dynamics, the same amount of data can be gained with far less energy consumed. This energy reduction offered by this sensor format's shortened minimum measurement window is a critical, enabling factor for monolithic CMOS sensors as powering sources are limited while subdermally implanted. Having observed that the pulsed electrochemical measurement and enzymatic portion of the device have sufficient long-term stability, it can next be investigated what is the long-term in vivo stability, which should be improved by the smaller, non-transdermal device format.

Oxygen availability can limit in vitro measurements but its average concentration in the capillary bed is a critical restricting factor for in vivo measurements, for which glucose flux limiting over-layers are added. One approach to ameliorate this external flux restriction is to more effectively recycle the available oxygen between the consumption reaction in the enzyme layer and the regeneration reaction at the electrode (H_2O_2 oxidation to regenerate O_2). Reducing the thickness of the enzyme layer allows for rapid transport between the enzyme and electrode, thereby maximizing the local effective oxygen concentration and bringing its availability more in balance with the glucose substrate. These oxygen-related issues stem from the described sensor being a 1st generation immobilized enzyme glucose sensor, but the functionalization approach described in this article is not limited to such. The enzyme immobilization process also prompts two other concerns that must be balanced (a) whether the polymerization of the GA has developed a sufficiently crosslinked matrix to adequately retain and stabilize the enzyme and (b) whether the polymerization has limited the enzyme catalytic activity by deforming or restricting the motion of domains of the enzyme[13,35]. Based on our experience and observation of others, a significant fraction of the deposited enzyme is inactivated in fabricated devices or at least does not contribute to measured signal during operation. Product losses by diffusion away from the electrode further reduce the overall transduced activity of the layer[36]. There are many field advancements in glucose sensor componentry that could be utilized in this planar structure such as conductive polymers, electrode modifications, and nanomaterials that have shown benefits in enzyme protection or fouling reduction. But the choice of these components is limited to their adaptability to efficient wafer-scale fabrication.

A thinner enzyme layer will provide a lower total available enzyme activity, which may result in the overall conversion rate deteriorating faster and having a shorter useful lifetime than that of a thicker layer. However this concern could be offset by reduced damage from H_2O_2 exposure[36] since the electrode being more proximal to the positions of all enzymes will therefore enable more complete consumption and a reduced maximum concentration. The minimum activity threshold for the enzyme layer is mainly controlled by parameters chosen in a flux limiting layer, so a complete answer cannot be given here. But if material consumption in sensor construction can be reduced, then cost reduction will also be possible.

Wafer-based biosensor fabrication can enable new or take advantage of existing wafer-scale probing methodologies for device quality assurance or calibration purposes. The semiconductor fabrication industry has benefited from the speed and decreased manipulations of parallel probing leading to reduced costs, which can also occur for wafer-based CGM construction. A key component of our development process was a 100 mm diameter wired wafer probing station as described in the data collection and methods. This enabled simultaneous data collection with a single fluidic system and without further wafer processing.

While the geometric control of a planar patterning process offers new opportunities, there are new challenges that are introduced. As the operation of the three electrodes employed can be modified or improved with techniques unique to the chemical reactions needed at the working, counter, and reference electrodes, it is possible to generate planarity issues that create non-uniformities when spincoating thin layers. And fabrication complexity can grow if the order of coating operations must be reconsidered due to severe surface height variations. Additionally, for cylindrically symmetric probes,

orientation within a sensing environment is insignificant. However, for planar devices, the direction of the sensing surface could affect the access to the sensing analyte, as might happen if the sensor was implanted between tissue layers with the sensor facing away from the more vascularized region. Pole-shaped sensors also have adhesion benefits as the polymer layers can wrap-around the circumference. For planar geometries, the chemical interactions and adhesion stabilities among subsequent layers must instead be carefully considered or adhesion-promoting features[37] must be intentionally introduced.

We have presented the fabrication of the enzyme biorecognition element layer, as this delicate biomolecule is the most outside the norm from a microfabrication perspective. However additional components, such as a flux-limiting layer, interference reduction material, or surface biocompatibility coating, must be integrated to perform in an ex vivo or in vivo environment. As these layers are composed of less sensitive materials (e.g. polyurethane, cellulose acetate, Nafion, polyethylene glycol, etc.[33,38,39]), we believe they will be less susceptible to processing condition incompatibility than the proteins of the biorecognition layer. The chemistry of immobilized GOx-BSA layers on platinum electrodes is fairly well understood but this implementation demonstrates new capabilities due to higher geometric control of enzyme layers in parallel sensor fabrication.

Besides the performance, the integration of glucose oxidase into a spincoat and photolithography process enables novel sensor geometries. Precisely controlling the height and lateral geometry of dropcoat enzyme layers is much more difficult than employing lithographically patterned liftoff due to droplet spreading and Marangoni processes while drying. Generalizing this approach, both the enzyme layer and subsequently fabricated structures could be laterally aligned to underlying features, providing new control for enzyme protection layers, or layers with additional functionality. The observed tolerance of the enzyme to photolithographic liftoff encourages the pursuit of additional avenues for enzymatic device fabrication, and in conjunction with GA vapor deposition may be applicable to patterned immobilization of other enzymes as well. The successful function of these thin coatings demonstrates that the total enzyme volume and thus reagent expense per device can and perhaps should be significantly reduced, which may aid cost-effectiveness for less-available enzyme dependent sensors. However, the described spincoating technique requires an excess of solution to be initially placed on the substrate before coating, but this becomes less significant as devices are more densely fabricated on the same substrate, as would occur on a CMOS wafer. Further study with height and lateral control of enzyme layers via additional thin film fabrication techniques is of future interest.

Conclusions

We have observed that a methodology of applying uniform layers of glucose oxidase via spincoating with subsequent vapor deposition of GA and patterning via liftoff is a viable approach to ease mass production of sensors while also improving performance. As shown, this technique can be employed directly on CMOS such that wireless sensors could be built purely by microfabrication processes. Spincoated enzyme layers have advantages in diffusion dynamics and substrate balance that increase their efficiency in collection of the enzyme product for conversion into a measurable signal. This fabrication process reduces the total enzyme consumed in sensor fabrication compared to the typically microns-thick dropcoat and dipcoat methods while also enabling nanometer-range enzyme thickness control. The consistency of these results demonstrates that building planar enzyme electrodes for future microfabricated CGM devices has the potential to reduce batch quality assurance efforts and calibration costs. The additional observations that the enzyme is compatible with solvent liftoff processing also suggests there are further, unexplored fabrication processes and geometries that may be viable for such enzymatic devices. The novel combination of microfabrication techniques and enzyme immobilization has been demonstrated to enable new monolithically built wireless CMOS CGM formats and may yield other designs in the future.

Author Contributions

Conceptualization, D.A, X.M., S.C., M.J., R.S., A.S., and P.P. investigation, D.A., X.M., S.C., M.J., S.L., C.A., J.C., A.A., and A.E. data curation and formal analysis D.A. and M.J. funding acquisition and advising A.S., A.E., P.P., and O.P. writing original draft, review, and editing D.A., R.S., P.P. and A.S.

Conflicts of interest

The following authors D. A., C. A., A. E., O. P., A. S. declare a competing financial interest concerning the overall enzymatic sensor platform and for consultation have received compensation fees/stock from, and their universities have licensed their patents to, an external corporation. The experiments reported in this work were completed prior to this conflict and the authors are not restricted in describing this work in publication.

Acknowledgements

The research reported here was supported in part by the Defense Advanced Research Projects Agency (DARPA) under Grant No. HR0011-15-2-0050. We gratefully acknowledge the critical support and infrastructure provided for this work by The Kavli Nanoscience Institute at Caltech.

Notes and references

1 P. D'Orazio, *Clinica Chimica Acta*, 2003, **334**, 41–69.
2 D. Grieshaber, R. MacKenzie, J. Vörös and E. Reimhult, *Sensors*, 2008, **8**, 1400–1458.
3 D. Bruen, C. Delaney, L. Florea and D. Diamond, *Sensors*, 2017, **17**, 1866.

4 G. Cappon, M. Vettoretti, G. Sparacino and A. Facchinetti, *Diabetes Metab J*, 2019, **43**, 383.
5 J. I. Joseph, G. Eisler, D. Diaz, A. Khalf, C. Loeum and M. C. Torjman, *Diabetes Technology & Therapeutics*, 2018, **20**, 321–324.
6 A. Koh, S. P. Nichols and M. H. Schoenfisch, *J Diabetes Sci Technol*, 2011, **5**, 1052–1059.
7 G. Rocchitta, A. Spanu, S. Babudieri, G. Latte, G. Madeddu, G. Galleri, S. Nuvoli, P. Bagella, M. Demartis, V. Fiore, R. Manetti and P. Serra, *Sensors*, 2016, **16**, 780.
8 A. Sassolas, L. J. Blum and B. D. Leca-Bouvier, *Biotechnology Advances*, 2012, **30**, 489–511.
9 T.-H. Wang, Z. Li, B. Liang, Y. Cai, Z. Wang, C. Yang, Y. Luo, J. Sun, X. Ye, Y. Chen and B. Zhao, in *2022 44th Annual International Conference of the IEEE Engineering in Medicine & Biology Society (EMBC)*, IEEE, Glasgow, Scotland, United Kingdom, 2022, pp. 4626–4630.
10 Y. Yu, T. Nguyen, P. Tathireddy, S. Roundy and D. J. Young, *Sensors and Actuators A: Physical*, 2022, **341**, 113574.
11 M. Mujeeb-U-Rahman, M. Honarvar Nazari and M. Sencan, *Biosensors and Bioelectronics*, 2019, **124–125**, 66–74.
12 F. R. Shu and G. S. Wilson, *Anal. Chem.*, 1976, **48**, 1679–1686.
13 R. A. Kamin and G. S. Wilson, *Anal. Chem.*, 1980, **52**, 1198–1205.
14 N. Kornienko, K. H. Ly, W. E. Robinson, N. Heidary, J. Z. Zhang and E. Reisner, *Acc. Chem. Res.*, 2019, **52**, 1439–1448.
15 C.-C. Chang, C.-L. Pai, W.-C. Chen and S. A. Jenekhe, *Thin Solid Films*, 2005, **479**, 254–260.
16 I. A. Ges and F. Baudenbacher, *Biosensors and Bioelectronics*, 2010, **25**, 1019–1024.
17 J. Kimura, A. Saito, N. Ito, S. Nakamoto and T. Kuriyama, *Journal of Membrane Science*, 1989, **43**, 291–305.
18 A. P. Soldatkin, A. V. El'skaya, A. A. Shul'ga, A. S. Jdanova, S. V. Dzyadevich, N. Jaffrezic-Renault, C. Martelet and P. Clechet, *Analytica Chimica Acta*, 1994, **288**, 197–203.
19 H. Teymourian, A. Barfidokht and J. Wang, *Chem. Soc. Rev.*, 2020, **49**, 7671–7709.
20 H. Lee, Y. J. Hong, S. Baik, T. Hyeon and D. Kim, *Adv Healthcare Materials*, 2018, **7**, 1701150.
21 G. S. Wilson and R. Gifford, *Biosensors and Bioelectronics*, 2005, **20**, 2388–2403.
22 J. J. Mastrototaro, K. W. Johnson, R. J. Morff, D. Lipson, C. C. Andrew and D. J. Allen, *Sensors and Actuators B: Chemical*, 1991, **5**, 139–144.
23 J. Lai, Y. Yi, P. Zhu, J. Shen, K. Wu, L. Zhang and J. Liu, *Journal of Electroanalytical Chemistry*, 2016, **782**, 138–153.
24 I. Migneault, C. Dartiguenave, M. J. Bertrand and K. C. Waldron, *BioTechniques*, 2004, **37**, 790–802.
25 L. D. Mell and J. T. Maloy, *Anal. Chem.*, 1975, **47**, 299–307.
26 M. Salem, Y. Mauguen and T. Prangé, *Acta Crystallogr F Struct Biol Cryst Commun*, 2010, **66**, 225–228.
27 A. Agarwal, A. Gural, M. Monge, D. Adalian, S. Chen, A. Scherer and A. Emami, in *2017 Symposium on VLSI Circuits*, IEEE, Kyoto, Japan, 2017, pp. C108–C109.
28 H. Angerstein-Kozlowska, B. E. Conway and W. B. A. Sharp, *Journal of Electroanalytical Chemistry and Interfacial Electrochemistry*, 1973, **43**, 9–36.
29 I. Katsounaros, W. B. Schneider, J. C. Meier, U. Benedikt, P. U. Biedermann, A. A. Auer and K. J. J. Mayrhofer, *Phys. Chem. Chem. Phys.*, 2012, **14**, 7384.
30 M. Koudelka-Hep, N. F. de Rooij and D. J. Strike, in *Immobilization of Enzymes and Cells*, ed. G. F. Bickerstaff, Humana Press, Totowa, NJ, 1997, pp. 83–85.
31 M. Mujeeb-U-Rahman, Meisam. H. Nazari, M. Sencan and W. V. Antwerp, *Sci Rep*, 2019, **9**, 17421.
32 A. P. F. Turner, I. Karube and G. S. Wilson, *Biosensors: Fundamentals and Applications*, Oxford University Press, 1987.
33 S. Vaddiraju, A. Legassey, Y. Wang, L. Qiang, D. J. Burgess, F. Jain and F. Papadimitrakopoulos, *J Diabetes Sci Technol*, 2011, **5**, 1044–1051.
34 D. C. Klonoff, *J Diabetes Sci Technol*, 2007, **1**, 130–132.
35 N. R. Mohamad, N. H. Marzuki, N. A. Buang, F. Huyop and R. A. Wahab, Biotechnology & Biotechnological Equipment, 2015, 29, 205–220.
36 K. Kleppe, *Biochemistry*, 1966, **5**, 139–143.
37 M. Liger, D. C. Rodger and Y.-C. Tai, in IEEE The Sixteenth Annual International Conference on Micro Electro Mechanical Systems, 2003. MEMS-03 Kyoto, 2003, pp. 602–605.
38 Yanan. Zhang, Yibai. Hu, G. S. Wilson, Dinah. Moatti-Sirat, Vincent. Poitout and Gerard. Reach, *Anal. Chem.*, 1994, **66**, 1183–1188.
39 S. P. Nichols, A. Koh, W. L. Storm, J. H. Shin and M. H. Schoenfisch, *Chem. Rev.*, 2013, **113**, 2528–2549.

Data for this article, including current-concentration measurements are available at CaltechDATA at https://doi.org/10.22002/r6fh3-9td32